Dark matter mass from relic abundance, an extra $U(1)$ gauge boson, and active-sterile neutrino mixing

Imtiyaz Ahmad Bhat[*] and Rathin Adhikari[†]

Centre for Theoretical Physics, Jamia Millia Islamia (Central University),
Jamia Nagar, New Delhi 110025, India

In a model with an extra $U(1)$ gauge to SM gauge group, we have shown the allowed region of masses of the extra gauge boson and the dark matter which is the lightest one among other right-handed Majorana fermions present in the model. To obtain this region, we have used bounds coming from constraints on active-sterile neutrino masses and mixing from various oscillation experiments, constraint on dark matter relic density obtained by PLANCK together with the constraint on the extra gauge boson mass and its gauge coupling recently obtained by ATLAS Collaboration at LHC. From the allowed regions, it is possible to get some lower bounds on the masses of the extra gauge boson and the dark matter and considering those values it is possible to infer what could be the spontaneous symmetry breaking scale of an extra $U(1)$ gauge symmetry.

I. INTRODUCTION

Although Standard Model (SM) has got tremendous success in describing various phenomena at the elementary particle level, but SM failed to account for two major experimental results, one related to the existence of dark matter (DM) [1] in the Universe and the other related to neutrino oscillation phenomena that require neutrinos to be massive and significant mixings among different flavors of neutrinos. To accommodate neutrino masses and a viable dark matter candidate something beyond SM is necessary. One such example is minimal extension of SM gauge group with an extra $U(1)_X$ gauge symmetry. Additional symmetries [2] either global or gauged are imposed which play the role in guaranteeing the stability of dark matter candidate. There are several $U(1)_X$ gauge extended models with minimal extension to the SM [3–5]. An important feature of these models is that in comparison to SM there is one extra neutral gauge boson. In general, there could be mixing of the extra gauge boson X with the SM Z boson, which results in the modification of neutral current phenomena. The Z pole data could be affected indirectly through such mixing and could shift the measured Z mass and its coupling to SM fermions. But nice agreement of the mass and coupling with SM predictions constrains such mixing to be lower than 1% [6].

*imtiyaz@ctp-jamia.res.in
†rathin@ctp-jamia.res.in

On the other hand, in cosmology to explain the rotational curves of the heavy massive body inside the galaxies, one need to propose the presence of dark matter [7,8]. Dark matter relic density has been constrained from PLANCK experiment [9].

$$\Omega_{\mathrm{DM}}h^2 = 0.1200 \pm 0.0012, \quad (1)$$

where Ω_{DM} is the density parameter for dark matter and $h = H_0/(100 \ \mathrm{km \ s^{-1} \ Mpc^{-1}})$. Recently, CMS and ATLAS [10–12] Collaborations at LHC have obtained stringent bound on the mass and gauge coupling associated with the extra $U(1)$ gauge boson. In the light of recent neutrino oscillation phenomena [13,14], there is a proposition of the presence of sterile neutrino apart from three active neutrinos. There are recent indications in the Fermilab experiment [15] about some nonzero mixing among active and sterile neutrinos with sterile neutrino mass in the eV scale [16].

In connection with these observational results, we have considered here an $U(1)$ gauge extended model [17], which contains dark matter fields and also can accommodate active-sterile neutrino masses and mixing. In this model, right-handed Majorana fermion is found to be a suitable candidate for dark matter as discussed later. There are some studies on the constraints on model parameters of $U(1)$ gauge extended models based on collider phenomenology and cosmological constraints [18]. However, in this work, we have shown in detail the allowed region in the dark matter mass m_ψ and the extra $U(1)$ gauge boson mass M_X plane. For that, we have considered PLANCK constraint on dark matter relic abundance. Besides, we consider constraints coming from active and sterile neutrino masses

and their mixing to find the allowed region. In the model considered here, the presence of appropriate active and sterile neutrino mass and their mixing requires the presence of appropriate range of mixing (angle θ) of dark matter with another right-handed Majorana fermion and their mass gap Δ as discussed later. In any extra $U(1)$ gauge model, the Majorana fermion (which is dark matter in our case) can be annihilated to SM fermion and antifermions through X boson as mediator. However, in our work, due to active-sterile mixing resulting in the nonzero value of θ, the coannihilation of dark matter with other Majorana fermion is also present. So the observed dark matter relic density will depend on both annihilation and coannihilation of dark matter in general in our work. With LHC constraint along with relic abundance constraint and constraint on Δ and θ (from neutrino oscillation data), we have also studied the possibility of lower bounds on mass of X boson and the dark matter mass and the corresponding $U(1)$ gauge coupling g_X.

Particularly, the allowed region is more for higher values of M_X and m_ψ. It is found that the allowed regions do not significantly vary with Δ values but are more sensitive to the variations of θ—the mixing of the dark matter with other heavy right-handed Majorana field considered in the model. All these analyses have been done considering $Z - X$ mixing to be zero at the tree level. Later on, we have shown that higher order corrections of this $Z - X$ mixing remain very small of the order of 10^{-5} and have been neglected.

In Sec. II, we have discussed the salient features of a model which is an $U(1)$ extension of the SM gauge group and the model can successfully explain active and sterile neutrino mass and mixing and also there is scope of dark matter. We have discussed the interaction of right-handed Majorana field in the mass basis with an extra gauge boson which will be useful for calculation of cross section for annihilation and coannihilation of dark matter. In Sec. III, using the experimental data on the active and sterile neutrino mass and their mixing, we have obtained the allowed region of the mass difference parameter Δ of dark matter with the next heavier right-handed Majorana fermion and their mixing angle θ. In Sec. IV, dark matter relic density has been studied, taking into account annihilation as well as coannihilation of dark matter with next heavier right-handed Majorana fermion going into final states of SM fermion antifermion pair. In Sec. V, in finding allowed model parameters, we have considered certain allowed values of Δ and θ as obtained in Sec. III from active and sterile neutrino mass and mixing. We have obtained the allowed parameter space for dark matter mass m_ψ, X boson mass M_X based on constraints coming from LHC, and relic abundance and also neutrino oscillation mass and mixing constraint corresponding to various Δ and θ values. In Sec. VI, we have discussed possible modification of $Z - X$ mixing after including higher order correction. In Sec. VII, we have concluded our work.

II. THE MODEL

Here we have considered a model [17] which is an $U(1)$ extension of SM, in which neutrino masses have been studied extensively and the mass of neutrinos has been connected to dark matter which is stabilized by a residual Z_2 symmetry of the spontaneously broken $U(1)$ gauge symmetry. The model has only one electroweak symmetry breaking doublet $\phi^{(+,0)}$ from which tree-level masses to quarks are obtained. Charged lepton masses are generated at one-loop level with dark matter as mediator. The three active and one sterile neutrino masses as well as mixing between active-sterile neutrinos have been generated through one loop. The model contains two heavy right-handed fermion triplet $\Sigma_{1R,2R}^{(+,0,-)}$ and three neutral singlet fermions N_R, S_{1R}, S_{2R}. These have been chosen so as to cancel all anomalies with each other. $U(1)_X$ gauge symmetry is spontaneously broken by singlet scalar $\chi_{1,2}^0$ and residual Z_2 symmetry is obtained. The other scalars are added to obtain masses for all fermions. There are two scalar doublets $\eta_{1,2}$—one couples to S_{1R} and other to two Σ's.

The fermionic and the scalar particles of the model are given in Tables I and II, respectively. Although there are several $U(1)$ charges corresponding to different fields but

TABLE I.   Fermion fields in the model.

Particle	$U(1)_X$	Z_2
$(u, d)_L$	n_1	$+$
u_R	$\frac{1}{4}(7n_1 - 3n_4)$	$+$
d_R	$\frac{1}{4}(n_1 + 3n_4)$	$+$
$(\nu, l)_L$	n_4	$+$
l_R	$\frac{1}{4}(-9n_1 + 5n_4)$	$+$
$\Sigma_{1R,2R}^{(+,0,-)}$	$\frac{3}{8}(3n_1 + n_4)$	$-$
N_R	$-\frac{3}{4}(3n_1 + n_4)$	$+$
S_{1R}	$\frac{1}{8}(3n_1 + n_4)$	$-$
S_{2R}	$\frac{5}{8}(3n_1 + n_4)$	$-$

TABLE II.   Scalar fields in the model.

Particle	$U(1)_X$	Z_2
$\phi^{(+,0)}$	$\frac{3}{4}(n_1 - n_4)$	$+$
$\eta_1^{(+,0)}$	$\frac{1}{8}(3n_1 - 7n_4)$	$-$
$\eta_2^{(+,0)}$	$\frac{1}{8}(9n_1 - 5n_4)$	$-$
χ_1^0	$\frac{1}{4}(3n_1 + n_4)$	$+$
χ_2^0	$\frac{3}{4}(3n_1 + n_4)$	$+$
χ_3^0	$\frac{1}{8}(3n_1 + n_4)$	$-$
χ_4^+	$\frac{3}{8}(n_1 - 5n_4)$	$-$
$\xi^{(++,+,0)}$	$\frac{1}{8}(9n_1 - 13n_4)$	$-$

using the anomaly cancellation equations all of them can be expressed in terms of the other two $U(1)$ charges n_1 and n_4, corresponding to quark doublet and lepton doublet, respectively. Under Z_2 symmetry, odd and even fields are specified in the last column of the above tables. The relevant Yukawa Lagrangian part of the model is

$$
\begin{aligned}
L \supset\ & h_{ij}^{\Sigma} \Sigma_{iR} \Sigma_{jR} \overline{\chi_2^0} + h_{12}^{S} S_{1R} S_{2R} \overline{\chi_2^0} + h_{11}^{S} S_{1R} S_{1R} \overline{\chi_1^0} \\
& + h_{23}^{N} N_R S_{2R} \chi_3^0 + h_{ij}^{\eta_2} \overline{\Sigma_{jR}^0} \nu_i \eta_2^0 + h_{i1}^{\eta_1} \overline{S_{1R}} \nu_i \eta_1^0 \\
& + h_{ij}^{\eta_2} l_{iL} \Sigma_{jR} \eta_2^+ + h_{ij}^{\xi} l_{iR} \Sigma_{jR} \xi^+ + h_{i1}^{\eta_1} l_{iL} S_{1R} \eta_1^+ \\
& + h_{i2}^{\chi} l_{iR} S_{2R} \chi_4^+.
\end{aligned}
$$

The first six terms are relevant for masses of Majorana fermions (shown in Table 1), and also these terms are relevant for active-sterile mixing of neutrinos at one-loop level as discussed later. Last four Yukawa interactions are relevant for charged lepton mass generation and have not been discussed here. $\chi_{1,2}^0$, which breaks $U(1)_X$ gauge symmetry spontaneously, give masses to $\Sigma_{1R,2R}^{(+,0,-)}$ and S_{1R}, S_{2R} through interaction as shown in first three terms above and so these scalars have even Z_2 parity. Also from these interactions, $U(1)_X$ charge of $\chi_{1,2}^0$ is specified by the corresponding $U(1)_X$ charge of triplet and singlet fermions as shown in the table. The active neutrinos get masses at one-loop level, through interactions shown in fifth and sixth terms in above interactions Lagrangian [17]. From $U(1)_X$ charges of the active neutrinos ν_i and the S_{1R}, S_{2R} fermions, it follows that the scalar fields in fifth and sixth terms are different from $\chi_{1,2}^0$. They do not have nonzero vacuum expectation value (vev). So $\eta_{1,2}^0$ is considered an odd under Z_2. The SM fields are even under Z_2. So from fifth and sixth terms in above interactions, it follows that $\Sigma_{1R,2R}^{(+,0,-)}$ and S_{1R}, S_{2R} are odd under Z_2. Interestingly, this oddness is decided by the $U(1)_X$ charge as discussed. Thus, these fermions could play the role of dark matter. From the required interactions for one-loop fermion masses for sterile neutrinos N_R and charged leptons, the Z_2 parity of other nonstandard model fields is decided [17]. N_R is the singlet neutrino which is massless at tree level. Mixing of N_R with active neutrinos as shown later in Fig. 1 and also the mass of N_R at one-loop level are obtained through interactions of N_R with S_{2R} and a scalar field χ_3. Here also scalar field different from $\chi_{1,2}$ is required because of the $U(1)_X$ charges of the fermions in this interaction and χ_3 which does not have nonzero vev is required to be odd under Z_2. Then N_R is required to be even under Z_2 and for that it is suitable for consideration as light sterile neutrino. The neutral scalars, odd under Z_2, in their mass basis have components, which are in general not electroweak singlets and as such they are not good dark matter candidate. This is because they will have too large cross section for their direct detection in underground experiments because of
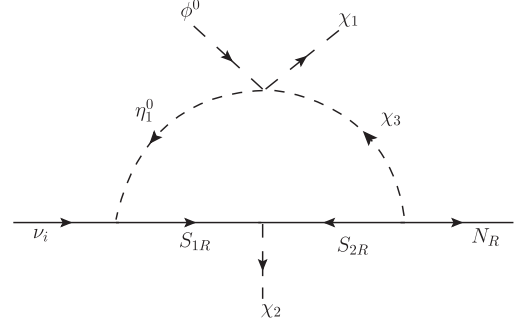

FIG. 1. One-loop active-sterile neutrino mixing [17].

their interactions with Z boson. $\Sigma_{1R,2R}^0$ as dark matter has been discussed in [19] and they do not play role in active-sterile neutrino mixing. However, $S_{1R,2R}$ could play the role of dark matter and also lead to active and sterile neutrino mixing as mediator at one loop and has been considered as possible dark matter candidate in our work.

We discuss in short the generation of mass of an extra gauge boson X and its mixing with SM neutral gauge boson Z. Let the vevs of various neutral scalars fields be $\langle \phi^0 \rangle = v_1$ and $\langle \chi_{1,2}^0 \rangle = u_{1,2}$, then the mass-squared elements, that determines mass for Z and X, are given as

$$
M_{ZZ}^2 = \frac{1}{2} g_Z^2 (v_1^2), \tag{2}
$$

$$
M_{ZX}^2 = M_{XZ}^2 = \frac{3}{8} g_Z g_X (n_1 - n_4) v_1^2, \tag{3}
$$

$$
M_{XX}^2 = \frac{1}{2} g_X^2 (3n_1 + n_4)^2 (u_1^2 + 9u_2^2) + \frac{9}{8} g_X^2 (n_1 - n_4)^2 v_1^2. \tag{4}
$$

Although in general, there is $Z - X$ mixing but it is expected to be very small so that electroweak precision measurements could be satisfied. The condition for no $Z - X$ mixing between neutral electroweak gauge boson and the extra $U(1)_X$ gauge boson is obtained for $M_{ZX}^2 = 0$ which gives $n_1 = n_4$. With this zero mixing consideration, the mass of the extra $U(1)_X$ gauge boson is

$$
M_{XX}^2 = \frac{1}{2} g_X^2 (4n_1)^2 (u_1^2 + 9u_2^2). \tag{5}
$$

Later on, we consider this zero mixing condition in dark matter relic density calculation.

Since the dark matter is Majorana in nature, its vector coupling with X boson is zero and it has only nonzero axial-vector coupling with X. The vector coupling g_{fv} and axial-vector coupling g_{fa} of the SM fermion fields with an extra gauge boson are given in Table III. These couplings are related to the chiral couplings [3] as follows:

$$
g_{f(v,a)} = \frac{1}{2} [\epsilon_L(f) \pm \epsilon_R(f)], \tag{6}
$$

TABLE III. Couplings of SM fermions with extra gauge boson X in terms of $U(1)$ charges n_1 and n_4. U and D are up and down type quarks, respectively.

	g_{fv}/g_X	g_{fa}/g_X
$l = e, \mu, \tau$	$\frac{9}{8}(n_4 - n_1)$	$\frac{1}{8}(n_4 - 9n_1)$
ν_l	$-\frac{n_4}{2}$	$-\frac{n_4}{2}$
U	$\frac{1}{8}(11n_1 - n_4)$	$\frac{3}{8}(n_1 - n_4)$
D	$\frac{1}{8}(5n_1 + 3n_4)$	$\frac{3}{9}(n_4 - n_1)$

where the chiral couplings $\epsilon_{L,R}(f)$ are g_X times $U(1)_X$ charges corresponding to left- and right-handed chiral fields as shown in Table III.

Let the mass eigenstates of the four Majorana fermions $S_{1R}, S_{2R}, \Sigma_{1R}^0, \Sigma_{2R}^0$ be ψ_k with mass m_{ψ_k}. The interaction basis $\psi_j'^T = [S_{1R}, S_{2R}, \Sigma_{1R}^0, \Sigma_{2R}^0]$ could be written in terms of this mass basis ψ_k as

$$\psi_j' = \sum_k z_{jk}\psi_k, \tag{7}$$

with $j, k = 1, \ldots 4$ where Σ_{1R}^0 and Σ_{2R}^0 are $SU(2)_L$ triplets and S_{1R} and S_{2R} are singlets. One of the lightest among ψ_k say, ψ_1 is a dark matter candidate in this model, which we assume that it mainly contains S_{1R} and S_{2R}. We consider ψ_2 as the next to lightest among these four mass eigenstates, and the masses m_{ψ_1} and m_{ψ_2} are not far apart.

In considering interactions of an extra gauge boson X with S_{1R} and S_{2R} in the mass basis of ψ_k, we are considering for simplicity that z_{ij} mixing matrix elements have nonzero 1–2 block with mixing angle θ which is decoupled from 3 to 4 block. Then the interaction can be written as

$$\sum_{i,j} \bar{S}_{iR}\gamma_\mu(g_{ij}\gamma^5)S_{jR}X_\mu$$

$$= (g_{S_{1R}a}\cos^2\theta + g_{S_{2R}a}\sin^2\theta)\bar{\psi}_1\gamma_\mu\gamma^5\psi_1 X_\mu$$

$$+ (g_{S_{1R}a}\sin^2\theta + g_{S_{2R}a}\cos^2\theta)\bar{\psi}_2\gamma_\mu\gamma^5\psi_2 X_\mu$$

$$+ \frac{1}{2}\sin 2\theta(g_{S_{1R}a} - g_{S_{2R}a})\bar{\psi}_1\gamma_\mu\gamma^5\psi_2 X_\mu$$

$$+ \frac{1}{2}\sin 2\theta(g_{S_{1R}a} - g_{S_{2R}a})\bar{\psi}_2\gamma_\mu\gamma^5\psi_1 X_\mu, \tag{8}$$

where $i, j = 1, 2$, $g_{S_{1R}a} = 5/8(3n_1 + n_4)g_X$, and $g_{S_{2R}a} = 1/8(3n_1 + n_4)g_X$. Here g_X is the gauge coupling for the extra gauge boson and the subscript a denotes that these are axial-vector couplings. The interactions shown in terms of mass basis will be useful in Sec. IV in our calculation of cross section of annihilation and coannihilation of dark matter.

III. ACTIVE AND STERILE NEUTRINO MASS AND MIXING

There are eight real scalar fields, spanning $\sqrt{2}\text{Re}(\eta_{1,2}^0)$, $\sqrt{2}\text{Im}(\eta_{1,2}^0)$, $\sqrt{2}\text{Re}(\chi_3^0)$, $\sqrt{2}\text{Im}(\chi_3^0)$, $\sqrt{2}\text{Re}(\xi^0)$, $\sqrt{2}\text{Im}(\xi_0)$, with mass eigenstate as ζ_l with mass m_l. These fields are present in the one-loop diagram giving radiative masses to active and sterile neutrinos. For details about the one-loop diagrams giving masses to active and sterile neutrinos, we refer readers to Ref. [17]. However, we have shown the one-loop diagram in Fig. 1 gives rise to active and sterile neutrino mixing.

Apart from three light active neutrinos, N_R plays the role of fourth neutrino as sterile in this model as mentioned earlier. The masses of active and sterile neutrinos are given as

$$(\mathcal{M}_\nu)_{ij}^{(2)} = \frac{h_{i1}^{\eta_2}h_{j1}^{\eta_2}}{16\pi^2}\sum_k(z_{3k})^2 m_{\psi_k}A_1$$

$$+ \frac{h_{i2}^{\eta_2}h_{j2}^{\eta_2}}{16\pi^2}\sum_k(z_{4k})^2 m_{\psi_k}A_2, \tag{9}$$

where $A_1 = \sum_l[(y_{2l}^R)^2 F(x_{lk}) - (y_{2l}^I)^2 F(x_{lk})]$ and $A_2 = \sum_l[(y_{2l}^R)^2 F(x_{lk}) - (y_{2l}^I)^2 F(x_{lk})]$ $\Sigma_{1R}^0 = \sum_k z_{3k}\psi_k$, $\Sigma_{2R}^0 = \sum_k z_{4k}\psi_k$, $\sqrt{2}\text{Re}(\eta_2^0) = \sum_l y_{2l}^R\zeta_l$, $\sqrt{2}\text{Im}(\eta_2^0) = \sum_l y_{2l}^I\zeta_l$, with $\sum_k(z_{3k})^2 = \sum_k(z_{4k})^2 = \sum_l(y_{2l}^R)^2 = \sum_l(y_{2l}^I)^2 = 1$, and $x_{lk} = m_l^2/m_{\psi_k}^2$ and $F(x_{lk}) = x_{lk}\ln x_{lk}/(x_{lk} - 1)$. Equation (9) is the contribution to the active neutrino masses from Σ_{1R} and Σ_{2R}.

Let $\bar{S}_{1R}\nu_i\eta_1^0$ coupling be $h_{i1}^{\eta_1}$, then the contribution to $\mathcal{M}_\nu$ is given by

$$(\mathcal{M}_\nu)_{ij} = \frac{h_{i1}^{\eta_1}h_{j1}^{\eta_1}}{16\pi^2}\sum_k(z_{1k})^2 m_{\psi_k}A, \tag{10}$$

where $A = \sum_l[(y_{1l}^R)^2 F(x_{lk}) - (y_{1l}^I)^2 F(x_{lk})]$, and $S_{1R} = \sum_k z_{1k}\psi_k$, $\sqrt{2}\text{Re}(\eta_1^0) = \sum_l y_{1l}^R\zeta_l$, $\sqrt{2}\text{Im}(\eta_1^0) = \sum_l y_{1l}^I\zeta_l$, with $\sum_k(z_{1k})^2 = \sum_l(y_{1l}^R)^2 = \sum_l(y_{1l}^I)^2 = 1$. We have assumed that the first contribution to active neutrino mass shown in Eq. (9) is somewhat lesser than the second contribution shown in Eq. (10) which gives masses to heavier neutrinos and the combination gives rise to appropriate mixing among different active neutrinos. We have considered only the mass scale for active neutrinos in our work and will be concerned with only Eq. (10).

Let $S_{2R}N_R\chi_3^0$ coupling be h_{23}^N, then the mass of sterile neutrino is given as

$$m_{NN} = \frac{h_{23}^N h_{23}^N}{16\pi^2}\sum_k(z_{2k})^2 m_{\psi_k}B, \tag{11}$$

where $B = \sum_l[(y_{3l}^R)^2 F(x_{lk}) - (y_{3l}^I)^2 F(x_{lk})]$ and $S_{2R} = \sum_k z_{2k}\psi_k$, $\sqrt{2}\text{Re}(\chi_3^0) = \sum_l y_{3l}^R\zeta_l$, $\sqrt{2}\text{Im}(\chi_3^0) = \sum_l y_{3l}^I\zeta_l$, with $\sum_k(z_{2k})^2 = \sum_l(y_{3l}^R)^2 = \sum_l(y_{3l}^I)^2 = 1$.

The active-sterile neutrino mixing is possible because of interaction $h^S_{12}S_{1R}S_{2R}\bar{\chi}^0_2$ as shown in Fig. 1, and nondiagonal mass matrix elements related to mixing in active-sterile neutrino mass matrix are given as

$$m_{\nu N} = \frac{h^{\eta_1}_{i1}(h^N_{23})}{16\pi^2}\sum_k z_{1k}z_{2k}m_{\psi_k}C,\qquad(12)$$

where $C = \sum_l[y^R_{1L}y^R_{3l}F(x_{lk}) - y^I_{1l}y^I_{3l}F(x_{lk}]$ and $\sum_k z_{1k}z_{2k} = \sum_l y^R_{1l}y^R_{3l} = \sum_l y^I_{1l}y^I_{3l} = 0$. A, B, and C are loop factors corresponding to the one-loop diagrams that give masses and mixing of neutrinos. Based on the recent global fit [20] of neutrino oscillation experiment with sterile neutrino in $3 + 1$ scheme, the best fit values are $\Delta m^2_{41} = 1.3$ eV^2, $|U_{e4}| = 0.1$, and $|U_{\mu 4}| \lesssim 10^{-2}$. Also, taking into account the cosmological constraint on sum of three active neutrino masses [21,22], we consider active neutrino masses, sterile neutrino mass, and active-sterile mixing as

$$(\mathcal{M}_\nu)_{ij} \sim 0.1 \text{ eV}, \qquad \mathcal{M}_{NN} \sim 1.14 \text{ eV},$$
$$\mathcal{M}_{\nu N} \sim 0.114 \text{ eV}.\qquad(13)$$

The product of the mixing matrix element and $m_{\psi k}$ which are present in Eqs. (10)–(12) can be rewritten in terms of the mixing angle θ and the mass gap parameter $\Delta = (m_{\psi_2} - m_{\psi_1})/m_{\psi_1}$ after we consider $z_{11} = \cos\theta$, $z_{12} = -\sin\theta$, $z_{21} = \sin\theta$, and $z_{22} = \cos\theta$. Following these, we can write

$$\sum_k z_{1k}z_{2k}m_{\psi_k} = \frac{\Delta m_{\psi_1}\sin 2\theta}{2}$$
$$\sum_k (z_{2k})^2 m_{\psi_k} = m_{\psi_1}(1 + \Delta\cos^2\theta)$$
$$\sum_k (z_{1k})^2 m_{\psi_k} = m_{\psi_1}(1 + \Delta\sin^2\theta).\qquad(14)$$

Using Eqs. (13) and (14) for active neutrino mass scale and the mixing of sterile neutrino U_{e4}, we can write Eqs. (10)–(12) in terms of Δ and θ parameters and can be written as

$$\frac{h^{\eta_1}_{11}h^{\eta_1}_{11}}{16\pi^2}m_{\psi_1}(1 + \Delta\sin^2\theta)\quad A \approx 0.1,\qquad(15)$$

$$\frac{h^N_{23}h^N_{23}}{16\pi^2}m_{\psi_1}(1 + \Delta\cos^2\theta)\quad B \approx 1.14,\qquad(16)$$

$$\frac{h^{\eta_1}_{11}h^N_{23}}{16\pi^2}m_{\psi_1}\left(\frac{\Delta\sin 2\theta}{2}\right)\quad C \approx 0.1.\qquad(17)$$

If we consider $\sum z^2 m_{\psi_k}$ of Eq. (14) of the order of 1 TeV and couplings $h \sim 0.1$, then from Eqs. (15)–(17), it is found that A, B, and C are in the range of 10^{-8} to 10^{-9}. However, considering the variation of two couplings $h^{\eta_1}_{11}$ and h^N_{23} in
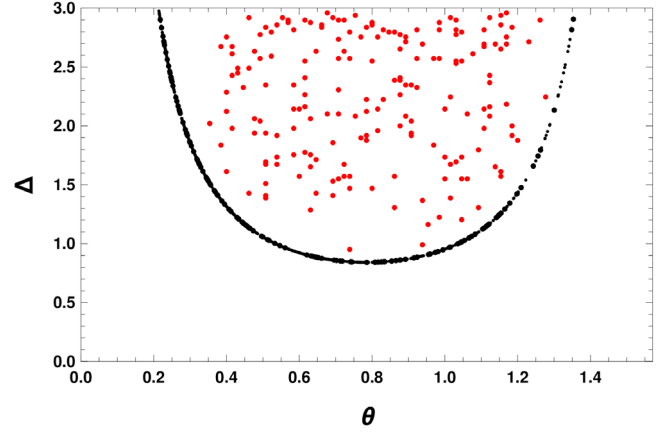

FIG. 2. Allowed region of Δ and θ (in radian) from active-sterile neutrino masses and mixing.

the range of 0.05–1 and A, B, and C in the range of $10^{-9} - 10^{-6}$ in Eqs. (15)–(17), we obtain the allowed region of θ and Δ as shown in Fig. 2. In Fig. 2, we consider two different conditions among A, B, and C: (1) $A = B = C$ and (2) $C < A$, B. The condition (1) gives the allowed almost semicircle outer line, whereas condition (2) gives region inside covered by that almost semicircle line. One may note here that A and B as mentioned just after Eqs. (10) and (11) are very similar in nature with the sum over the product of the mixing matrix elements of y being 1 for both A and B, whereas for C as mentioned just after Eq. (12) due to orthogonality condition the sum over the product of the mixing matrix elements of y vanishes. Due to this difference, C is expected to be lesser than both A and B. In that sense, we should consider the proper allowed region of Δ and θ as that given by the region inside the almost semicircle line in Fig. 2 and $\Delta \geq 1$ is found to be preferred.

For active and sterile neutrino mixing, one important conclusion follows from both Figs. 1 and 2 is that there is necessarily nonzero mixing θ between S_{1R} and S_{2R}; otherwise, there will be zero contribution from Fig. 1. Figure 2, however, shows apart from nonzero mixing, the simultaneous constraint on both θ and Δ. These imply that apart from annihilation of two dark matter fields (ψ_1) into SM fermion and antifermion pair, there is coannihilation of dark matter field ψ_1 with other next heavier Majorana field ψ_2 through the interactions mentioned in Eq. (8).

IV. DARK MATTER (ψ_1) RELIC DENSITY

Relic density is obtained from the Boltzmann equation [23] governing the evolution of number density of the DM with the thermally averaged cross section for the process $\psi_1\psi_1 \to f\bar{f}$. The Boltzmann equation is written as

$$\dot{n}_{\psi_1} + 3Hn_{\psi_1} = \langle\sigma v\rangle((n^{\text{eqb}}_{\psi_1})^2 - n^2_{\psi_1}),\qquad(18)$$

where n_{ψ_1} is the number density and $n_{\psi_1}^{\text{eqb}}$ is thermal equilibrium number density of the DM particle. H is Hubble expansion rate of the Universe, and $\langle \sigma v \rangle$ is the thermally averaged cross section for the process $\psi_1 \psi_1 \to f \bar{f}$ and is given by [24]

$$\langle \sigma v \rangle = \frac{1}{8m_{\psi_1}^4 T K_2^2(m/T)} \int_{4m_{\psi_1}^2}^{\infty} \sigma(s - 4m_{\psi_1}^2) \sqrt{s} K_1(\sqrt{s}/T) ds,$$

(19)

where K_1, K_2 are modified Bessel functions of first and second kinds, respectively. Here s is the center of mass energy squared. The thermally averaged cross section can be expanded in powers of relative velocity of two dark matter particle to be scattered and is written as $\langle \sigma v \rangle = a + bv^2$. Numerical solution of the above Boltzmann equation gives [25]

$$\Omega_{\psi_1} h^2 \approx \frac{1.04 \times 10^9 x_f}{M_{\text{pl}} \sqrt{g_*}(a + 3b/x_f)},$$

(20)

where $x_f = m_{\psi_1}/T_f$, T_f is the freeze-out temperature, g_* is the number of relativistic degrees of freedom at the time of freeze-out. x_f can be found from

$$x_f = \ln \frac{0.038 M_{\text{Pl}} m_{\psi_1} \langle \sigma v \rangle}{g_*^{1/2} x_f^{1/2}}.$$

(21)

We assume ψ_1 to be lighter than ψ_2 and it plays the role of dark matter. The lighter ψ_1 will be pair annihilated to SM fermions and antifermions through the extra gauge boson mediator but not Z boson as we are considering $Z - X$ mixing to be zero. This pair annihilation has been considered above. However, it could also coannihilate with ψ_2. Both annihilation and coannihilation cross sections could control the relic abundance of the dark matter ψ_1 [26,27]. To take into account coannihilation, we discuss the necessary modifications in the Boltzmann equation below.

If the mass difference between ψ_1 and ψ_2 is very large, ψ_2 will be out of thermal equilibrium much earlier than ψ_1 and coannihilation will not play a significant role in the evolution of the number density of ψ_1. However, we consider the case where the mass difference may not to be too large. In that case, we consider the annihilation as well as the coannihilation channel in the coupled Boltzmann equation to find out the evolution of the number density of ψ_1 and hence find the relic density of dark matter. Using the formalism of Ref. [26], we can reduce the system of two Boltzmann equations governing number densities n_1 and n_2 of ψ_1 and ψ_2, respectively, into one Boltzmann equation which governs the evolution of $n = n_1 + n_2$ in the early Universe as given below.

$$\dot{n} = -3Hn - \sum_{i,j=1}^{2} \langle \sigma_{ij} v \rangle ((n_i n_j - n_i^{\text{eq}} n_j^{\text{eq}}),$$

(22)

where $\langle \sigma_{ij} v \rangle$ is the thermally averaged scattering cross section for the process $\psi_i \psi_j \to f \bar{f}$. This equation can be further simplified as

$$\dot{n} = -3Hn - \sum_{i,j=1}^{2} \langle \sigma_{\text{eff}} v \rangle ((n^2 - (n^{\text{eq}})^2),$$

(23)

where σ_{eff} is given as

$$\sigma_{\text{eff}} \approx \sum_{i,j=1}^{2} \sigma_{ij} \frac{g_i g_j}{g_{\text{eff}}^2} (1 + \Delta_i)^{3/2} (1 + \Delta_j)^{3/2} \exp^{-x(\Delta_i + \Delta_j)}.$$

(24)

Here $x = m_{\psi_1}/T$ and $\Delta_i = \frac{m_{\psi_i} - m_{\psi_1}}{m_{\psi_1}}$. Then $\Delta_1 = 0$ by definition. Later on, Δ_2 is written as Δ. g_i is the internal degrees of freedom of the interacting particles and g_{eff} is defined as

$$g_{\text{eff}} = \sum_{i=1}^{2} g_i (1 + \Delta_i) 3/2 \exp^{-x\Delta_i}.$$

(25)

For comparison with the general weakly interacting massive particle formulas, we have Taylor expanded the thermally averaged cross sections,

$$\langle \sigma_{ij} v \rangle = a_{ij} + b_{ij} v^2; \qquad \langle \sigma_{\text{eff}} v \rangle = a_{\text{eff}} + b_{\text{eff}} v^2,$$

(26)

where a_{eff} and b_{eff} are given by

$$a_{\text{eff}} \approx \sum_{i,j=1}^{2} a_{ij} \frac{g_i g_j}{g_{\text{eff}}^2} (1 + \Delta_i)^{3/2} (1 + \Delta_j)^{3/2} \exp^{-x(\Delta_i + \Delta_j)},$$

(27)

$$b_{\text{eff}} \approx \sum_{i,j=1}^{2} b_{ij} \frac{g_i g_j}{g_{\text{eff}}^2} (1 + \Delta_i)^{3/2} (1 + \Delta_j)^{3/2} \exp^{-x(\Delta_i + \Delta_j)}.$$

(28)

The phase space integration part for all the process of $\psi_i \psi_j \to f \bar{f}$ is almost same for cross section calculation, and the difference in the cross sections is mainly due to the strength of couplings g_{ij} in which both the indices i, j run from 1 to 2. Because of this, we can write

$$\frac{\sigma_{11}}{|g_{11}|^2} \approx \frac{\sigma_{12}}{|g_{12}|^2} \approx \frac{\sigma_{21}}{|g_{21}|^2} \approx \frac{\sigma_{22}}{|g_{22}|^2}.$$

(29)

Using this approximation σ_{eff} in Eq. (24), it can be written in terms of σ_{11} as

$$\sigma_{\text{eff}} = \frac{g_i g_j}{g_{\text{eff}}^2} \left[1 + 2r_{12} \frac{g_{12}^2}{g_{11}^2} + r_{22} \frac{g_{22}^2}{g_{11}^2} \right] \sigma_{11}.$$

(30)

Here, $r_{12} = (1 + \Delta)^{3/2} e^{-x\Delta}$, $r_{22} = (1 + \Delta)^3 e^{-2x\Delta}$, and $\Delta = (m_{\psi_2} - m_{\psi_1})/m_{\psi_1}$ and σ_{11} is annihilation cross section of $\psi_1 \psi_1 \to f\bar{f}$, and $\langle \sigma_{11} v \rangle$ can be Taylor expanded in the form of $a_{11} + b_{11} v^2$. For Majorana fermions $g_i = g_j = 2$ (internal degrees of freedom) and from Eq. (8), the couplings involved in these annihilation and coannihilation channels are

$$g_{11} = g_{S_{1R}a} \cos^2\theta + g_{S_{2R}a} \sin^2\theta$$
$$g_{22} = g_{S_{2R}a} \cos^2\theta + g_{S_{1R}a} \sin^2\theta$$
$$g_{12} = g_{21} = \frac{1}{2} \sin 2\theta (g_{S_{1R}a} - g_{S_{2R}a}). \tag{31}$$

In the presence of coannihilation of dark matter ψ_1 with ψ_2, Eqs. (20) and (21) will be modified as

$$\Omega_{\psi_1} h^2 \approx \frac{1.04 \times 10^9 x_f}{M_{\rm pl} \sqrt{g_*} (a_{11} I_a + 3 b_{11} I_b / x_f)}, \tag{32}$$

where

$$I_a = \frac{x_f}{a_{11}} \int_{x_f}^\infty x^{-2} a_{\rm eff} dx \ \text{ and } \ I_b = \frac{2x_f^2}{b_{11}} \int_{x_f}^\infty x^{-3} b_{\rm eff} dx \tag{33}$$

and x_f can be obtained from

$$x_f = \ln \frac{0.038 M_{\rm Pl} m_{\psi_1} \langle \sigma_{\rm eff} v \rangle}{g_*^{1/2} x_f^{1/2}}. \tag{34}$$

Following [28], the annihilation cross section of Majorana fermion to SM $f\bar{f}$ through s channel mediated by X boson is given as

$$\sigma_{11} = \frac{n_c}{12\pi s[(s - M_X^2)^2 + M_X^2 \Gamma_X^2]} \sum_f \sqrt{\frac{1 - 4m_f^2/s}{1 - 4m_{\psi_1}^2/s}}$$
$$\times \left[g_{fa}^2 g_{11}^2 \left(4m_{\psi_1}^2 \left[m_f^2 \left(7 - \frac{6s}{M_X^2} + \frac{3s^2}{M_X^4} \right) - s \right] \right. \right.$$
$$\left. \left. + s(s - 4m_f^2) \right) + g_{fv}^2 g_{11}^2 (s + 2m_f^2)(s - 4m_{\psi_1}^2) \right], \tag{35}$$

where $n_c = 3$ when f stands for quarks and $n_c = 1$ when f stands for leptons and $s \approx 4m_{\psi_1}^2 + m_{\psi_1}^2 v^2$. In the above equation, $\Gamma_X = \Gamma_{X_1} + \Gamma_{X_2}$ is the total decay width of an extra gauge boson X, where Γ_{X_1} is the decay width of the extra gauge boson X to SM fermion antifermion pair and Γ_{X_2} is the decay width of the extra gauge boson decaying to $\psi_i \psi_j$ Majorana fermions,

$$\Gamma_{X_1} \equiv \sum_f \Gamma(X \to f\bar{f})$$

$$= \sum_f \frac{n_c M_X}{12\pi S} \sqrt{1 - \frac{4m_f^2}{M_X^2}} \left[g_{\rm fa}^2 \left(1 - \frac{4m_f^2}{M_X^2} \right) + g_{\rm fv}^2 \left(1 - 2\frac{m_f^2}{M_X^2} \right) \right]$$

$$\Gamma_{X_2} = \sum_{i,j} \Gamma(X \to \psi_i \bar{\psi}_j) = \sum_{i,j} \frac{M_X g_{ij}^2}{12\pi S} \left[1 - \frac{4m_{\psi_i} m_{\psi_j}}{M_X^2} \right]^{3/2}, \tag{36}$$

where $S = 1$ (2) for (in)distinguishable final state particles. In the notation of Eq. (26), $\langle \sigma_{11} v \rangle = a_{11} + b_{11} v^2$, where

$$a_{11} = \frac{n_c g_{fa}^2 m_f^2 g_{11}^2 m_{\psi_1}}{24\pi [(M_X^2 - 4m_{\psi_1}^2)^2 + M_X^2 \Gamma_X^2]}$$
$$\times \sqrt{1 - \frac{m_f^2}{m_{\psi_1}^2}} \left(12 - 96\frac{m_{\psi_1}^2}{M_X^2} + 192\frac{m_{\psi_1}^4}{M_X^4} \right),$$

$$b_{11} = a_{11} \left[-\frac{1}{4} + \frac{m_f^2}{8(m_{\psi_1}^2 - m_f^2)} - \frac{M_X^4 - 16M_X^2 m_{\psi_1}^2 + 48m_{\psi_1}^4}{4((M_X^2 - 4m_{\psi_1}^2)^2 + M_X^2 \Gamma_X^2)} \right.$$
$$\left. + \frac{\left(-4 + 2\frac{g_{fv}^2}{g_{fa}^2} + 4\frac{m_{\psi_1}^2}{m_f^2} + 4\frac{g_{fv}^2 m_{\psi_1}^2}{g_{fa}^2 m_f^2} - 24\frac{m_{\psi_1}^2}{M_X^2} + 96\frac{m_{\psi_1}^4}{M_X^4} \right)}{\left(12 - 96\frac{m_{\psi_1}^2}{M_X^2} + 192\frac{m_{\psi_1}^4}{M_X^4} \right)} \right]. \tag{37}$$

Mass M_X of the extra gauge boson in the above expressions is given by Eq. (5), and g_{11} corresponds to axial-vector coupling as follows from Eqs. (31) and (8).

V. ALLOWED REGION OF DARK MATTER MASS, X BOSON MASS, AND ITS GAUGE COUPLING

Large Hadron Collider (LHC) operating at $\sqrt{s} = 13$ TeV has searched for new phenomena [10–12] which are resonant as well as nonresonant and in which the final state is dilepton/dijet. This is a robust test for all theories beyond the SM. ATLAS at LHC has obtained the allowed region of coupling g_X of quarks and leptons with an extra gauge boson mass M_X in Fig. 4 of [10] and Fig. 5(a) of [11] at 95% confidence level. However, these two figures in Refs. [10,11] do not differ too much. We have considered the allowed region of g_X and M_X in Fig. 5(a) of Ref. [11] in our numerical analysis. g_X coupling in our paper is related to coupling γ' of this figure as $g_X \approx 0.463\gamma'$.

For our numerical analysis, $U(1)$ charges are fixed by considering $n_1 = n_4 = 1/\sqrt{2}$ (normalizing $n_1^2 + n_4^2 = 1$) which satisfies zero mixing condition of an extra gauge boson X with SM Z boson. We have considered two values of Δ as 1 as 1 and 2 and also different values of θ as 0.4, $\pi/4$, and 1.2 as allowed by Fig. 2.
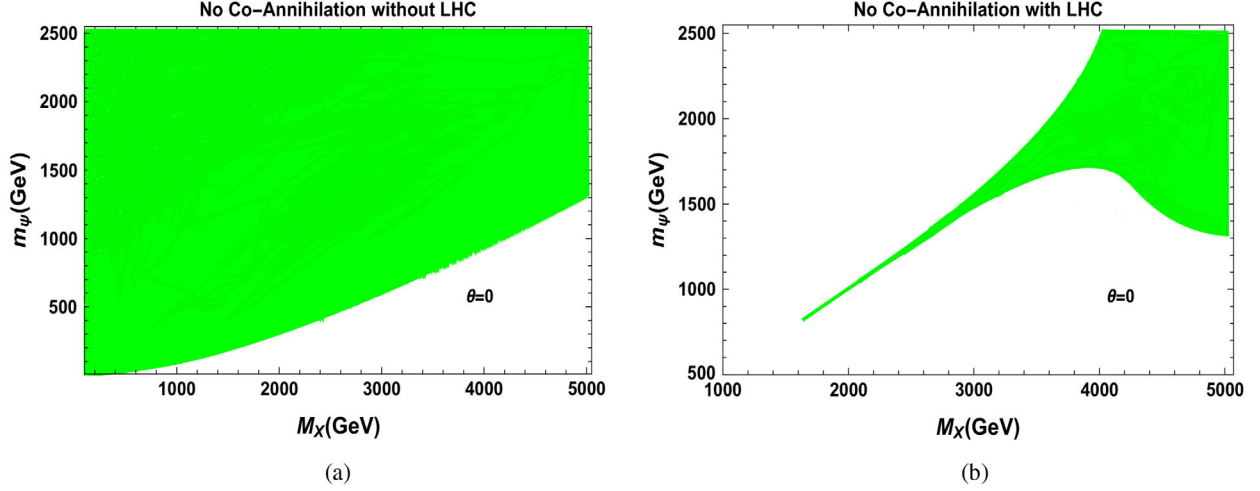
FIG. 3.   Allowed green region in the M_X and m_ψ plane for the no coannihilation channel satisfies PLANCK relic density bound $\Omega h^2 \in (0.1188, 0.1212)$. (a),(b) correspond to no LHC constraints and LHC constraints on M_X and g_X, respectively.

In the later part, we have used the symbol m_ψ for the dark matter mass m_{ψ_1}. In Fig. 3, we first show the allowed region in $M_X - m_\psi$ plane for only the annihilation channel ($\psi_1 \psi_1 \to f \bar{f}$) but no coannihilation of dark matter fermion. As discussed earlier, this will not in general correspond to active and sterile neutrino mixing in the model considered by us because of the no coannihilation channel. For comparing the allowed region with and without LHC constraint, as shown in Fig. 3, we have considered the variation of g_X over the range (0.005–0.7), m_ψ up to 2.5 TeV, and M_X up to 5 TeV, as this is the range considered by LHC. The other two parameters θ and Δ are zero as this figure is only for the annihilation case. In plotting Fig. 3(a), we have considered only the constraint coming from relic abundance on dark matter from PLANCK 2018 $\Omega h^2 \in$ (0.1188, 0.1212) [9]. But, in Fig. 3(b), we have also considered the constraint on g_X and M_X given by ATLAS Collaboration [10,11] at LHC. Comparing Figs. 3(a) and 3(b), one can see that LHC constraint significantly reduces the allowed region of dark matter mass for lower values of $M_X < 4000$ GeV and for further lower M_X the allowed range of dark matter mass m_ψ is further constrained with respect to no LHC constraint in Fig. 3(a). For M_X lesser than about 1600 GeV and m_ψ lesser than about 700 GeV, it is difficult to get any allowed region.

In Fig. 4, apart from considering the constraint coming from relic abundance on dark matter from Planck 2018, we have also considered the coannihilation channel along with the annihilation channel for the dark matter as required for satisfying active and sterile neutrino masses and mixing. As discussed in Sec. III, the preferred allowed region of Δ and θ is shown in Fig. 2 inside the almost semicircular line. We consider in Fig. 4 different values of Δ and θ based on Fig. 2. But no LHC constraint has been imposed.

One can see after including the coannihilation channel for all cases in Fig. 4 there is a significant constraint on

allowed dark matter mass for any M_X value in comparison to Fig. 3(a) with no coannihilation for which $\theta = 0$. A significant change has come mainly due to nonzero θ value considered in Fig. 4 as the coupling g_{ij} of $\psi_i \psi_j X$ as shown in Eqs. (8) and (31) changes with the change in θ values. As for example, for $\theta = 0$, g_{12} is zero. The second term (related to the process $\chi_1 \chi_2 \to f\bar{f}$) in $\sigma_{\rm eff}$ in Eq. (30) is zero for $\theta = 0$, whereas this is nonzero for nonzero θ value. Δ plays the role of more suppression of the effect of this process on $\sigma_{\rm eff}$ for its higher values. The third term (related to the process $\chi_2 \chi_2 \to f\bar{f}$) in $\sigma_{\rm eff}$ is more exponentially suppressed than the second term for higher Δ values. So, if Δ values are increased further than those considered in Fig. 4, there will be further lesser effect from second and third terms in $\sigma_{\rm eff}$. For smaller Δ values much lesser than 1, there would have been more effect from the second and third terms in $\sigma_{\rm eff}$ in Eq. (30) due to coannihilation. One may note however that active and sterile neutrino mixing constrains both Δ and θ simultaneously, as shown in Fig. 2, and for Δ less than about 1, there is no allowed θ value for coannihilation to occur. In Figs 4(a) and 4(b), we have chosen $\Delta = 2$, $\theta = \pi/4$ and $\Delta = 1$m $\theta = \pi/4$, respectively, to see how much the allowed region in $M_X - m_\psi$ plane changes due to this variation of Δ for same θ value. In fact, one can see that the change is insignificant as both the figures are almost the same. However, it is also expected that there will be change in $\sigma_{\rm eff}$ to some extent for variations in m_{ψ_1} values also as follows from (30) but this is subject to details of the Boltzman equations and the corresponding freeze-out temperature T. In Figs 4(c) and 4(d), we have changed θ values to 0.4 and 1.2, respectively, with Δ fixed at 2. Comparing Figs. 4(b)–4(d), it is found that the allowed region changes significantly with such variations of θ value.

For freeze-out temperature $T \sim m_\psi$, one can see from Eqs. (30) and (31) and (8) that $\sigma_{\rm eff}$ increase with increase in
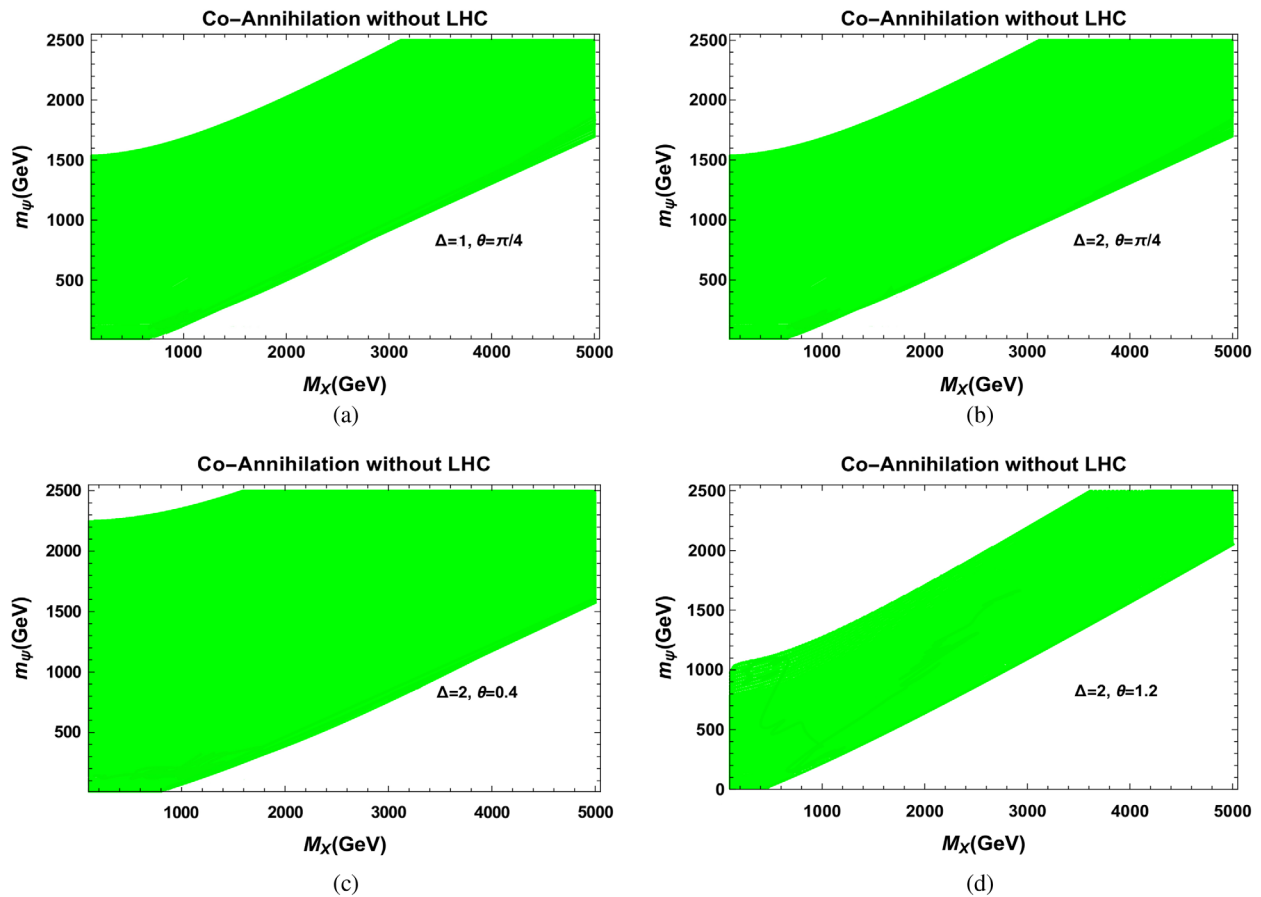
FIG. 4. Allowed green region in the M_X and m_ψ plane for coannihilation channels with different choices of $\Delta = 2$, $\theta = 0.4$, $\pi/4$, 1.2, and $\Delta = 1$, $\theta = \pi/4$ (in radian). The allowed region satisfies PLANCK relic density bound $\Omega h^2 \in (0.1188, 0.1212)$.

θ values and the constraint on relic density in Eq. (32) reduces the allowed parameter space of dark matter mass for any M_X value further with increase in θ values. In Fig. 4(c), the chosen θ value is relatively smaller and the allowed region of M_X and m_ψ is more than that in 4(b) and 4(d).

Figure 5 is like previous Fig. 4 but with LHC constraint on M_X and g_X imposed. Because of that, the allowed region for lower M_X is very much reduced while for higher M_X above 4000 GeV there is more allowed region. This feature is similar to Fig. 3(b). Like Figs. 4(a) and 4(b), the allowed region is almost the same in Figs. 5(a) and 5(b). This shows that for $\Delta \geq 1$ with same value of θ there is an insignificant change in the allowed region for the same reason as discussed in the context of previous figure. With the variation of θ again, the similar feature appears like in the previous figure—namely for higher θ value there is lesser allowed region. In Fig 5(c), the chosen θ value is relatively smaller and the allowed region of M_X and m_ψ is more than that of in (b) and (d). Due to LHC constraint in Fig. 5, for different cases there are different lower bounds on M_X and m_ψ depending on different set of values of Δ and θ. This feature is similar to Fig. 3(b). For higher θ value, the lower bound values for both these parameters

increases to some extent with lesser allowed region. As, for example, in Fig. 5(d), the lower bound on M_X and m_ψ is at about 2000 and 900 GeV, respectively, which are relatively higher than those in Fig. 5(c).

Based on Figs. 3(b) and 5, we have shown the lower values of M_X and m_ψ in Table IV. The g_X value as mentioned in the table has been taken from the data file corresponding to the lower values of M_X and m_ψ related to these figures. The vev of χ_1 and χ_2 fields has been evaluated using the tree-level relationship of the model as given in Eq. (5) to get an understanding of the possible scale of an extra $U(1)$ spontaneous symmetry breaking. For the coannihilation channel, the vev of χ_1 and χ_2 field (assuming them to be equal) is around 10 TeV, whereas for the no coannihilation channel it is around 17 TeV.

VI. HIGHER ORDER EFFECT ON $Z - X$ MIXING

Now we address the question of $Z - X$ mixing due to higher order corrections coming from one-loop Feynman diagrams as shown in Fig. 6. The contribution from the fermions in the loop is proportional to axial-vector coupling only and as such for our choices of $n_1 = n_4$ (corresponding to tree-level zero $Z - X$ mixing) the axial-vector coupling
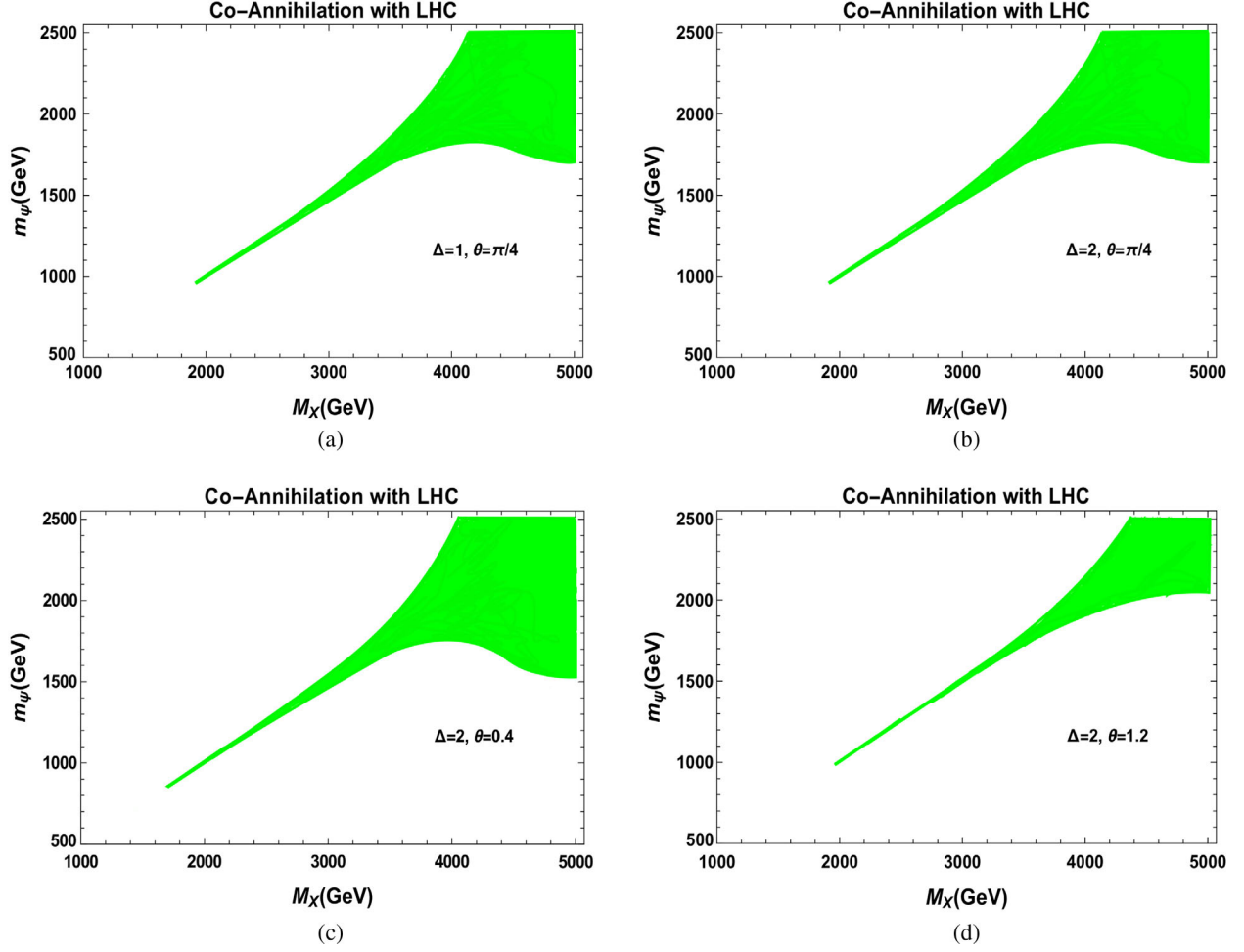
FIG. 5. Allowed green region in the M_X and m_ψ plane for coannihilation channels with different choices of $\Delta = 2$, $\theta = 0.4$, $\pi/4$, 1.2 and $\Delta = 1$, $\theta = \pi/4$ (in radian). The allowed region satisfies LHC bound and PLANCK relic density bound $\Omega h^2 \in (0.1188, 0.1212)$.

vanishes for quarks as shown in Table III giving zero contribution to M_{ZX}^2 due to quarks in the loop. The dark fermion is not possible in the loop diagram as there is no coupling of Z with dark fermion due to zero $Z - X$ mixing considered at the tree level. One-loop correction to M_{ZX}^2 will have main contribution coming from τ lepton in the loop because of nonzero axial coupling for our choice of $n_1 = n_4$. The general expression for one-loop correction to M_{ZX}^2 can be written as

$$\delta M_{ZX}^2 \approx -\frac{1}{4\pi^2} \sum_f c_A g_Z g_{f_a} m_f^2$$
$$\times \left(-\frac{1}{\epsilon} + \gamma_e - \log(4\pi) + \log\frac{m_f^2}{\mu^2} \right). \quad (38)$$

Here g_Z is the SM neutral coupling constant and c_A is the coefficient depending on the particular SM fermion coupling with Z boson, and g_{f_a} is the axial-vector coupling of SM fermions with X boson as given in Table III.

TABLE IV. Lower values of M_X and m_ψ and corresponding g_X and vevs.

Δ	θ	g_X	M_X(GeV)	m_ψ(GeV)	$\sqrt{u_1^2 + 9u_2^2}$(TeV)	$u_1 = u_2$(TeV)
2	0.4	0.021	1702	850	40.523	12.814
	$\pi/4$	0.035	1910	960	27.285	8.628
	1.2	0.025	1970	990	39.40	12.45
1	$\pi/4$	0.035	1910	960	27.285	8.628
No coannihilation		0.015	1645	825	54.833	17.33
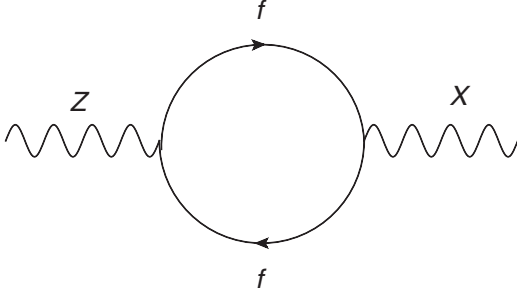
FIG. 6.   One-loop Feynman diagram contributing to $Z - X$ mixing.

For completeness, we give the result for one-loop correction to M_{XX}^2. As we do not know its tree-level value from the model, this correction will not be used in our numerical computation of mixing. The main contribution to it will come from dark fermion ψ_1 and ψ_2 and also from top quark as fermion in the loop and the one-loop corrections to M_{XX}^2 due to dark matters are given by

$$\delta M_{XX}^2(\psi_1) \approx -\frac{M_{XX}^2}{12\pi^2}\left(\frac{g_{11}^2}{4} - \frac{3m_{\psi_1}{}^2}{8M_{XX}^2}\right)$$
$$\times \left(\frac{1}{\epsilon} - \gamma_e + \log(4\pi) - \log\frac{m_{\psi_1}{}^2}{\mu^2}\right). \quad (39)$$

Contribution to δM_{XX}^2 due to ψ_2 in the fermionic loop will have similar expression like above with the replacement of g_{11} by g_{22} and m_{ψ_1} by m_{ψ_2}. One-loop correction to M_{XX}^2 due to top quark and other fermions is given by

$$\delta M_{XX}^2(\text{SM fermion}) \approx -\frac{N_c M_{XX}^2}{12\pi^2}\sum_f\left(\frac{(g_{f_v}^2 + g_{f_a}^2)}{4} - \frac{3m_f{}^2}{8M_{XX}^2}\right)$$
$$\times \left(\frac{1}{\epsilon} - \gamma_e + \log(4\pi) - \log\frac{m_f{}^2}{\mu^2}\right),$$
$$(40)$$

in which g_{f_v} and g_{f_a} are given explicitly in terms of n_1, n_4 and g_X in Table III and $N_c = 3$ for quarks and $N_C = 1$ for leptons as well as for dark fermions.

We have followed $\overline{\text{MS}}$ scheme for numerical evaluation of $Z - X$ mixing. The corresponding mixing angle θ_{ZX} is given by

$$\tan 2\theta_{ZX} = \frac{2(M_{ZX} + \delta M_{ZX})}{M_{XX} - M_{ZZ}}. \quad (41)$$

In M_{ZX}, the one-loop correction is included for numerical evaluation. As an example to find a possible value of mixing, we have considered $g_X = 0.035$, $M_{XX} = 1910$ GeV, $m_\psi = 960$ GeV as one set of values from Table IV for lowest possible values of M_X and m_ψ for which mixing could be little bit larger and have used M_{ZZ} as the experimentally measured value of Z boson as $91.18(\text{GeV})$. For such choices, we find $\theta_{ZX} = 6 \times 10^{-5}$, which is quite a small number and much lesser than the possible experimental bound [6] of about 10^{-2}, and one

may consider this mixing to be almost zero with $n_1 = n_4$ even after higher order correction.

VII. CONCLUSION

Apart from Planck data constraint on relic abundance and LHC constraint on an extra $U(1)$ gauge boson mass and its gauge coupling, we have taken into account the possible constraints coming from active, sterile neutrino masses and their mixing from different oscillation experiments to find the allowed region in M_X and m_ψ plane. In the extra $U(1)$ gauge model considered by us, the oscillations constraints—particularly active-sterile mixing have led to the requirement of nonzero mixing θ between dark matter ψ_1 with the other heavy right-handed Majorana fermion ψ_2. This has led to the consideration of the coannihilation channel for the dark matter. Also, the oscillation data constrain the allowed region of θ and Δ as shown in Fig. 2. The allowed region in M_X and m_ψ plane is found to be reduced for the coannihilation channel with respect to the no coannihilation channel. Particularly, the allowed region with the coannihilation channel is sensitive to θ value as shown in Sec. V and for higher θ values with same Δ value there is lesser allowed region in the M_X and m_ψ plane.

The other important thing is that particularly with the LHC constraint, in general there is some kind of lower bound on both M_X and m_ψ as shown in Figs. 3(b) and 5 in Sec. V. Using the corresponding g_X value from Table IV as followed from our numerical analysis for such lower values of M_X and m_ψ and using the tree-level relationship of the model as given in Eq. (5), which connects vevs of χ_1 and χ_2 with the mass of an extra gauge boson M_X, we get an understanding of the possible scale of the extra $U(1)$ spontaneous symmetry breaking as shown in Table IV. However, for higher values of M_X, such specific conclusion is difficult to obtain because of multiple possible values of M_X, m_ψ, and g_X in the allowed region. The numerical analysis has been done considering zero $Z - X$ mixing at the tree level with $n_1 = n_4$ which alters insignificantly even after including higher order corrections and satisfies various phenomenological low energy constraints. With the improvement on the constraint on the extra $U(1)$ gauge boson mass and its gauge coupling from LHC experiments, the allowed region in M_X and m_ψ plane could be further reduced and the lower bounds on M_X and m_ψ could be further higher.

[1] G. Bertone, D. Hooper, and J. Silk, Phys. Rep. **405**, 279 (2005).

[2] J. C. Montero and V. Pleitez, Phys. Lett. B **675**, 64 (2009); E. Ma and R. Srivastava, Phys. Lett. B **741**, 217 (2015); S. Singirala, R. Mohanta, and S. Patra, Eur. Phys. J. Plus **133**, 477 (2018); V. De Romeri, E. Fernandez-Martinez, J. Gehrlein, P. A. N. Machado, and V. Niro, J. High Energy Phys. 10 (2017) 169; E. Bertuzzo, P. A. N. Machado, Z. Tabrizi, and R. Zukanovich Funchal, J. High Energy Phys. 11 (2017) 004; M. D. Campos, D. Cogollo, M. Lindner, T. Melo, F. S. Queiroz, and W. Rodejohann, J. High Energy Phys. 08 (2017) 092.

[3] P. Langacker, Rev. Mod. Phys. **81**, 1199 (2009).

[4] D. Suematsu and Y. Yamagishi, Int. J. Mod. Phys. A **10**, 4521 (1995); M. Cvetic and S. Godfrey, [hep-ph/9504216]; A. Leike, Phys. Rep. **317** (1999); M. Cvetic and P. Langacker, arXiv:hep-ph/9707451; D. A. Demir, Phys. Rev. D **59** (1998) 015002; J. L Diaz-Cruz, J. M. Hernandez-Lopez, and J. A. Orduz-Ducuara, J. Phys. G **40**, 125002 (2013).

[5] E. Ma, Phys. Rev. D **73**, 077301 (2006).

[6] J. Erler, P. Langacker, S. Munir, and E. Rojas, J. High Energy Phys. 08 (2009) 017; F. del Aguila, J. de Blas, and M. Perez-Victoria, J. High Enrgy Phys. 09 (**2010**) 033; R. Diener, S. Godfrey, and I. Turan, Phys. Rev. D **86**, 115017 (2012); J. Erler and P. Langacker, Phys. Lett. B **456**, 68 (1999).

[7] F. Zwicky, Helv. Phys. Acta **6**, 110 (1933); Gen. Relativ. Gravit. **41**, 207 (2009).

[8] D. N. Spergel et al. (WMAP Collaboration), Astrophys. J. **148** (2003) 175; M. Tegmark et al. (SDSS Collaboration), Phys. Rev. D **69**, 103501 (2004).

[9] N. Aghanim et al. (Planck Collaboration), arXiv:1807.06209.

[10] M. Aaboud et al. (ATLAS Collaboration), Phys. Rev. D **96**, 052004 (2017).

[11] M. Aaboud et al. (ATLAS Collaboration), J. High Energy Phys. 10 (2017) 182.

[12] A. M. Sirunyan et al. (CMS Collaboration), Phys. Lett. B **769**, 520 (2017); **772**, 882(E) (2017).

[13] M. C. Gonzalez-Garcia, M. Maltoni, and T. Schwetz, Nucl. Phys. **B908**, 199 (2016).

[14] M. H. Ahn et al. (K2K Collaboration), Phys. Rev. D **74**, 072003 (2006).

[15] P. Adamson et al. (NOvA Collaboration), Phys. Rev. D **96**, 072006 (2017).

[16] A. A. Aguilar-Arevalo, Phys. Rev. Lett. **121**, 221801 (2018); A. M. Sirunyan et al. (CMS Collaboration), J. High Energy Phys. 08 (2018) 130; 06 (2018) 120.

[17] R. Adhikari, D. Borah, and E. Ma, Phys. Lett. B **755**, 414 (2016).

[18] N. Okada, S. Okada, and D. Raut, Phys. Rev. D **100**, 035022 (2019); T. Nomura and H. Okada, Eur. Phys. J. C **78**, 189 (2018); N. Okada and S. Okada, Phys. Rev. D **95**, 035025 (2017); S. Singirala, R. Mohanta, S. Patra, and S. Rao, J. Cosmol. Astropart. Phys. 11 (**2018**) 026; Z. L. Han and W. Wang, Eur. Phys. J. C **78**, 839 (2018); M. Escudero, S. J. Witte, and N. Rius, J. High Energy Phys. 08 (2018) 190.

[19] E. Ma and D. Suematsu, Mod. Phys. Lett. A **24**, 583 (2009).

[20] M. Dentler, Á. Hernández-Cabezudo, J. Kopp, P. A. N. Machado, M. Maltoni, I. Martinez-Soler, and T. Schwetz, J. High Energy Phys. 08 (2018) 010.

[21] S. Vagnozzi, S. Dhawan, M. Gerbino, K. Freese, A. Goobar, and O. Mena, Phys. Rev. D **98**, 083501 (2018).

[22] S. Roy Choudhury and S. Choubey, J. Cosmol. Astropart. Phys. 09 (2018) 017.

[23] M. Beltran, D. Hooper, E. W. Kolb, and Z. C. Krusberg, Phys. Rev. D **80**, 043509 (2009).

[24] P. Gondolo and G. Gelmini, Nucl. Phys. **B360**, 145 (1991).

[25] E. W. Kolb and M. S. Turner, Front. Phys. **69**, 1 (1990).

[26] K. Griest and D. Seckel, Phys. Rev. D **43**, 3191 (1991).

[27] M. Cannoni, Eur. Phys. J. C **76**, 137 (2016).

[28] A. Berlin, D. Hooper, and S. D. McDermott, Phys. Rev. D **89**, 115022 (2014).